JGR Space Physics

RESEARCH ARTICLE
10.1029/2020JA027829

The Acceleration of Lunar Ions by Magnetic Forces in the Terrestrial Magnetotail Lobes

Xin Cao[1], Jasper Halekas[1], Andrew Poppe[2], Feng Chu[1], and Karl-Heinz Glassmeier[3]

[1]Department of Physics and Astronomy, University of Iowa, Iowa City, IA, USA, [2]Space Sciences Laboratory, University of Californi, Berkeleya, Berkeley, CA, USA, [3]Institut für Geophysik und Extraterrestrische Physik, Technische Universität Braunschweig, Braunschweig, Germany

Key Points:
- ARTEMIS observes accelerated lunar ions in the magnetotail lobes
- Magnetic field perturbations occur contemporaneously with accelerated lunar ions
- The acceleration of lunar ions in the lobes is dominantly driven by magnetic forces

Supporting Information:
- Supporting Information S1

Correspondence to:
X. Cao,
xin-cao@uiowa.edu

Citation:
Cao, X., Halekas, J., Poppe, A., Chu, F., & Glassmeier, K.-H. (2020). The acceleration of lunar ions by magnetic forces in the terrestrial magnetotail lobes. *Journal of Geophysical Research: Space Physics*, *125*, e2020JA027829. https://doi.org/10.1029/2020JA027829

Received 17 JAN 2020
Accepted 4 MAY 2020
Accepted article online 18 MAY 2020

Abstract In order to study the acceleration of ions originating from the tenuous exosphere and surface of the Moon, we analyzed data from the ElectroStatic Analyzer (ESA) and Flux Gate Magnetometer (FGM) carried by the Acceleration, Reconnection, Turbulence, and Electrodynamics of Moon's Interaction with the Sun (ARTEMIS) spacecraft. Previous investigations have modeled the acceleration of lunar ions by the motional electric field of the surrounding plasma. However, in the terrestrial magnetotail, where the lunar ion density can equal or even exceed the ambient plasma density, other forces may play an important role in the tenuous plasma environment. Determining what forces govern lunar ion motion is important in understanding their interaction with the ambient plasma in the unique environment of the magnetotail. Based on a detailed analysis of two individual ARTEMIS observations, we find that magnetic pressure and magnetic tension forces may play an important role in accelerating the lunar ions.

1. Introduction

The Moon has a tenuous exosphere, which is mainly composed of neutral particles released from the lunar surface (Stern, 1999). There are multiple processes through which neutral particles in the exosphere and on the lunar surface are transformed to heavy ions with the same mass, including photoionization, photon, and electron-stimulated desorption, charge exchange, impact ionization (Huebner & Mukherjee, 2015; McGrath et al., 1986; Sarantos et al., 2012), and micrometeoroid bombardment (Halekas et al., 2011; Hartle & Killen, 2006; Horányi et al., 2015; Stern, 1999). Studying these lunar ions can help us understand the fundamental physical processes that occur at the Moon and the linkages between the lunar surface, the exosphere, and the ambient plasma environment.

The lunar plasma environment when the Moon orbits through regions with appreciable plasma density, such as the solar wind, the magnetospheric plasma sheet, or the magnetosheath, is predominately controlled by the flow of the ambient plasma, which has much higher density than that of the lunar ions in these regions. Futaana et al. (2003) reported the ring-like velocity distribution of protons near the dayside of the Moon. Saito et al. (2010) further discussed the ions originating from the Moon surface/exosphere. In a dense flowing magnetized plasma such as the solar wind, newborn ionized particles are picked up and accelerated by a $-v \times B$ motional electric field during the so-called pickup process (Halekas et al., 2012, 2013, 2015; Hartle et al., 2011; Hilchenbach et al., 1992; Mall et al., 1998; Sarantos et al., 2012; Yokota et al., 2009). In this process, lunar ions are accelerated by the motional electric field and subsequently experience $E \times B$ drift motion (Halekas et al., 2012). Halekas et al. (2012) utilized ARTEMIS data to constrain the dominant mass range of lunar pickup ions to ~20–45 amu by studying pickup ion trajectories in the solar wind.

In the terrestrial magnetotail lobes, the pickup process has also been considered as a potential mechanism for the acceleration of lunar ions (Poppe et al., 2012; Zhou et al., 2013), with the near-surface sheath electric field also playing a role (Poppe et al., 2013; Tanaka et al., 2009). Poppe et al. (2012) estimated the lower limit of lunar pickup ions to be ~24 amu, using a model of the combined pickup and sheath electric field acceleration. Zhou et al. (2013) showed that the average mass of lunar pickup ions was ~28 amu, based on the plasma quasi-neutrality requirement and the fact that ARTEMIS instruments underestimate the ion density.

In contrast to the ambient solar wind, in the terrestrial magnetotail lobes the density of lunar ions is commonly comparable to or even larger than the density of the ambient lobe plasma (Halekas

et al., 2018). This condition invalidates the test-particle approximation commonly used to describe pure $-v \times B$ pickup, since the ambient plasma flow cannot provide the momentum required to pick up the lunar ions. The lobes in the magnetotail therefore provide a unique environment to investigate the dynamics of the lunar ions, since the local plasma environment can be appreciably perturbed by the presence of the lunar ions. In this scenario, the magnetic perturbations produced by the interaction with the ambient flow may provide the dominant forces that accelerate newborn ions (Vasyliūnas, 2016). In the multifluid's perspective, ion kinetic behaviors such as the gyration of different ion fluids can be captured (Alvarez-Laguna et al., 2018; Huang et al., 2018; Rubin et al., 2014). For instance, the two fluid description of plasma is derived from the Vlasov equation (Bellan, 2008). The momentum equation of the αth ion in the multifluid model can be described as follows (Sauer et al., 1996; Toth et al., 2010; Zieger et al., 2015):

$$\frac{\partial \rho_\alpha \boldsymbol{u}_\alpha}{\partial t} + \nabla \cdot (\rho_\alpha \boldsymbol{u}_\alpha \boldsymbol{u}_\alpha + I p_\alpha) = n_\alpha q_\alpha (\boldsymbol{u}_\alpha - \boldsymbol{u}_+) \times \mathbf{B} + \frac{n_\alpha q_\alpha}{n_e e} (\mathbf{J} \times \mathbf{B} - \nabla p_e) + S_{\rho_\alpha \boldsymbol{u}_\alpha}, \quad (1)$$

where ρ_α and $\boldsymbol{u}_\alpha$ are the ion mass density and velocity, respectively, p_α and $p_e$are ion and electron pressures, n_α is the ion number density, q_α and e are the charge of ion and electron, $\mathbf{J}$ and $\mathbf{B}$ are the current density and the magnetic field, $\boldsymbol{u}_+ = \sum_\alpha n_\alpha q_\alpha \boldsymbol{u}_\alpha / (e n_e)$, and $S_{\rho_\alpha \boldsymbol{u}_\alpha}$ is arbitray source term caused by electron-ion collisions, charge exchange, etc. Since the plasma is relatively cold in the magnetotail lobes, the pressure terms are negligible compared to other source terms. Due to the plasma quasi-neutrality requirement and the small ambient proton density in the lobes as we discussed, $n_e \approx n_h + n_p \approx n_h$ in the model, where n_h represents the heavy ion density, and on the right side of the equation above the second term dominates compared to the first term. Therefore, the acceleration of ions is dominantly controlled by the $J \times B$ force. Besides, we can also estimate the minor effect of the first term if considering a nominal nonzero n_p. For instance, considering the nominal ambient ion density that ARTEMIS measured beyond the period when lunar ions were detected and the lunar ions density during the period when lunar ions were detected, n_p/n_h~1/10, and the lunar ions were accelerated to ~20 km/s, the ratio of the second term to the first term on the right-hand side of the equation is much larger than 1 (the method of calculating the second term magnetic force will be described in the next section). Therefore, the first term is reasonably small to be discarded in the model equation in this scenario.

Since this set of equations shows that for heavy mass-loading (in contrast to "test-particle pickup") there are appreciable forces on the ambient plasma as well as the newly ionized particles, which ultimately lead to the slowdown of the ambient flow and the development of a magnetic disturbance structure, particularly in the sub-Alfvénic background flow of the magnetotail lobes. These structures have previously been observed around other moons in the solar system within their parent body magnetospheres, for example, Ganymede and Io in Jupiter's magnetosphere (Kivelson et al., 1997; Linker et al., 1998) and Rhea in Saturn's magnetosphere (Simon et al., 2012).

In this paper, we suggest that, in contrast to the conventional pick-up process driven by the $-v \times B$ motional electric field in the solar wind, in the terrestrial magnetotail lobes the interaction between ambient and lunar plasma should lead to the formation of a disturbance region, which is created by the mass loading process. This structure has been referred as an Alfven wing in other Moons which have similarly plasma-induced field disturbance, for example, Enceladus (Jia et al., 2010), Titan (Sillanpää & Johnson, 2015), even though their cause is different from the traditional Alfven wing as originally discussed by Drell et al. (1965) and Neubauer (1980). The associated magnetic perturbation and resultant magnetic forces (magnetic tension and magnetic pressure) should play an important role in the acceleration of the lunar ions. In section 2, we introduce the instrumentation of ARTEMIS for the observations in this study. In section 3, we utilize data from the ARTEMIS Electrostatic Analyzer (ESA) (McFadden et al., 2008) and Fluxgate Magnetometer (FGM) (Auster et al., 2008) instruments to investigate the disturbed structure of the mass loading region formed by the interaction between the lunar and the ambient plasma, for two events reported by Poppe et al. (2012) and Zhou et al. (2013, 2014). For each of the two events, we investigate the lunar ions' acceleration by the magnetic pressure and tension forces, which are generated by the perturbed local environment of a mass loading structure and compare the results with the velocity of lunar ions measured by ARTEMIS. Finally, in section 4, we summarize our study and outline future work.

2. Instrumentation and Methodology

The ARTEMIS mission is a two-spacecraft redeployment of Time History of Events and Macroscale Interactions during Substorms (THEMIS) mission, which originally consisted of five spacecraft (Angelopoulos, 2011). The two redeployed spacecraft were renamed P1 and P2 and finally transferred into lunar orbit. In this study, we utilize data from two of the on-board instruments: ESA and FGM. The ESA measures the ion distribution from a few eV to 25 keV and electron distribution from a few eV up to 30 keV (McFadden et al., 2008). The FGM measures the vector magnetic field at a cadence of ~4 s minimum.

The coordinate system utilized in this study is Selenographic Solar Ecliptic (SSE), in which the $+X_{SSE}$ axis is directed toward the Sun from the center of the Moon, the $+Z_{SSE}$ axis points toward the ecliptic north pole, and the $+Y_{SSE}$ axis completes the right-handed system. The two probes of ARTEMIS follow elliptical orbits around the Moon. The orbits of the probes are near-equatorial, with aposelenes of ~20,000 km and periselenes that vary from tens to hundreds of km. A dominant positive B_x component was observed during the two events, indicating that the Moon was in the north tail lobe.

Since the ESA, which measures flux as a function of energy per charge, does not discriminate between ions of different mass, heavy ions' speed is overestimated by a factor of $\sqrt{M/q}$, where M is the atomic mass number. Since the particle flux is correctly measured regardless of ion mass, the ion density is underestimated by a factor of $\sqrt{M/q}$ (McFadden et al., 2008; Zhou et al., 2013). Poppe et al. (2012) calculated that the lower limit of lunar ions' mass is 24 amu when the Moon was in the magnetotail lobes. Zhou et al. (2013) further estimated that the average mass is 28 amu in this scenario. In this study, we therefore utilize a correction factor of $\sqrt{28} \approx 5.29$. Based on the assumption that plasma is quasi-neutral, the charge density of ions and electrons should be equal (Zhou et al., 2013),

$$n_e = n_{i^-\text{corrected}} = \sqrt{M}\cdot\left(n_i - n_p\right) + n_p, \tag{2}$$

where n_e is the electron density, n_i is the ARTEMIS-measured ion density, n_p is the background proton density, and $n_{i\ -\ \text{corrected}}$ is the corrected overall ion density, which sums the heavy ion density and the background proton density. The electron density is also checked from the electric field spectra, which is consistent with lobe ESA measurement for our result.

Similarly, the heavy ion velocity can be estimated by considering the measured overall ion flux equal to the summation of the heavy ion flux and the background proton flux,

$$n_h\cdot V_h + n_p\cdot V_p = n_i\cdot V_i, \tag{3}$$

according to the density relationship shown as Equation 2, the flux equation can be transformed to as follows:

$$\sqrt{M}\cdot\left(n_i - n_p\right)\cdot V_h + n_p\cdot V_p = n_i\cdot V_i, \tag{4}$$

where V_h is the heavy ion velocity, the V_p is the background proton velocity, and V_i is the nominal ion velocity ARTEMIS measured. Here, n_p can be estimated by the average value that the ion ESA (iESA) measured during the window before and after the heavy lunar ions are detected. However, due to the large positive spacecraft potential, low-energy protons cannot reach the spacecraft, and this measurement is unreliable. Furthermore, the nominal ambient ion density that ARTEMIS measured beyond the period when lunar ions were detected is also much smaller than the ion density during the period when lunar ions were detected. Therefore, we simply set n_p to zero, which we found had no significant impact on the calculation of the heavy ion velocity for the first-order approximation. Similarly, ARTEMIS is incapable of directly measuring the small bulk plasma speed in the ambient lobe environment (Poppe et al., 2012) because of the positive spacecraft potential. However, since the second term in Equation 4 is neglected because n_p is set to zero, we therefore expect the perpendicular component of the ambient background convective velocity does not significantly affect the result for the first-order approximation in this equation. In order to accurately measure the lunar ion velocity, the background noise which contaminates the velocity measurement of the lunar ions should be excluded. The method is calculating the

moments of lunar ions by restricting their exclusive velocity direction and energy range, the details of which will be described in the next section.

Since the orbit of ARTEMIS is almost on the equator of the Moon, and the trajectory when the satellite P1 or P2 flew by the dayside near surface of the Moon is approximately perpendicular to the background magnetic field during the events we will discuss in the next section, these events provide an opportunity to track and investigate a component of the lateral magnetic forces and velocities of lunar ions. We can estimate the magnetic tension and magnetic pressure along the 1-D flyby trajectory of a satellite above the dayside of the Moon, which gives us a first-order approximation of the magnetic forces that accelerate the lunar ions in this direction. The tangential component of the magnetic force $J \times B$ can be divided into two parts: magnetic tension $(B \cdot \nabla_T)B_T/\mu_0$ and magnetic pressure $-\nabla_T(B^2/2\mu_0)$, where ∇_T represents the differential delta or nabla operator calculated along the trajectory of the ARTEMIS satellite near the Moon. In the dayside area where ARTEMIS crossed, ∇_T approximates the nabla operator along the SSE Y direction, perpendicular to the magnetic field. The magnetic tension term is generated when the field line is curved and the tension force tends to bend the line back until the line becomes straight. In contrast, the pressure term is generated when the magnitude of the magnetic field is inhomogeneous, and the pressure force acts from high to low magnetic pressure regions (Kamide & Chian, 2007). Since the time window of the variation of the detected plasma is about 10 min during the events in this study, we calculate the divergence and gradient across 10 min when we measure the magnetic forces. In order to confine the magnetic forces to the specific dimension along the spacecraft trajectory, during the calculation we project the vectors to the tangential direction of the local trajectory. For instance, $B = (B_T, B_N)$, where B_T and B_N, respectively, represent the tangent and the normal components of the magnetic field at a local point on the trajectory. Since we focus on the dimension along the satellite trajectory, the normal component B_N was negligible when calculating the magnetic tension term. Meanwhile, we assume that the initial perpendicular velocity of lunar ions was zero. By comparing the estimated lunar ion velocity that would be produced by acceleration from zero by the magnetic forces with the ARTEMIS-measured ion velocity, we can investigate how large the impact of the magnetic field perturbation on the lunar ion's acceleration is.

3. Results and Discussion

The Moon orbited through the magnetotail lobe ~60 Earth radii (R_E) downstream from the Earth during two events that took place on 11 November 2011 and 29 October 2012 (Poppe et al., 2012; Zhou et al., 2014). The geomagnetic K_p index during both events was less than 1, indicating quiet geomagnetic conditions. The magnetic field was dominated by the B_x component, the positive value of which indicates that the Moon was in the northern lobe region. On 11 November 2011, ARTEMIS P2 flew by the dayside of the Moon from the dawnside to duskside during 10:45–11:35 UTC. On 29 October 2012, ARTEMIS P1 flew by the dayside of the Moon from the duskside to dawnside during 04:45–05:45 UTC.

Figure 1 reveals the overall structure of the magnetic field fluctuation near the Moon, combined with the trajectories of ARTEMIS' fly-by on 11 November 2011 and 29 October 2012, respectively. The left plots show the X-Z plane on which the Moon is observed from the dawnside. The solid black curves represent the disturbed field structure caused by the mass loading upstream of the Moon, and the dashed curves represent the downstream field structure in the wake. The right plots show the X-Y plane on which the mass loading of the Moon is observed from the side view. The mass loading disturbance structure is shifted from the lunar center since the ionosphere is concentrated above the surface of the dayside.

3.1. The 11 November 2011 Event

We utilized ion data from ESA and magnetic field data from FGM to investigate the ion velocity and magnetic field perturbations along the dayside trajectory. Figure 2a (the upper subfigure of Figure 2) shows ARTEMIS P2 original measurements of ion velocity and magnetic field difference from ARTEMIS P1 made during 10:45–11:35 UTC on 11 November 2011, when P1 was far from the Moon (~[2, −7.5, 0.8] R_U in SSE coordinates) and P2 was above the dayside of the Moon. The Moon is at ~[−60, −7, 2] R_E in GSE coordinates, where R_E is the radii of the Earth. Because of the quiet geomagnetic conditions, the magnetic field data from P1 can be treated as an unperturbed background. In another word, the two ARTEMIS probes measure the same magnetic field far from the Moon, but the Moon perturbs the magnetic field near the Moon, which

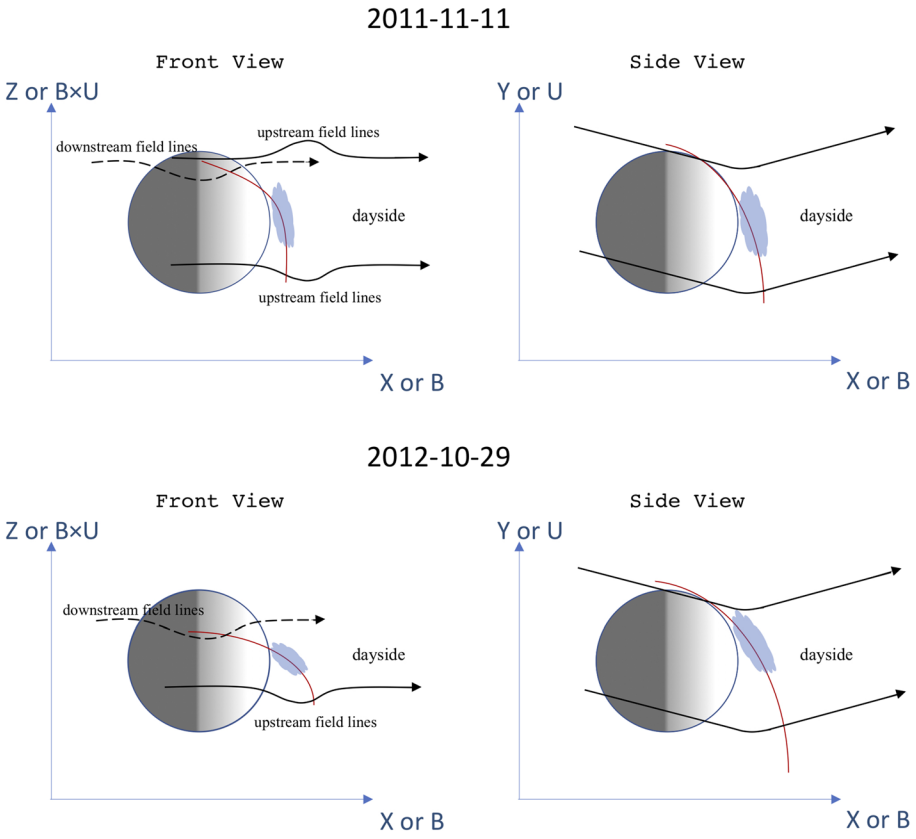

Figure 1. The overall magnetic field structure caused by mass loading near the Moon. The black curves represent the disturbed field structure. In each left plot, the solid and dashed curves represent the upstream and downstream structure, respectively. The red curve represents the trajectory of ARTEMIS. The blue-shaded regions are the locations where the accelerated ions were observed, which does not necessarily represent the entire regions of mass loading.

is revealed by the difference between P1 and P2 measurements when one probe flew by the Moon. The orbits and vector quantities are converted from Solar Selenocentric Ecliptic (SSE) to a coordinate system such that the *X*-*Y* plane in the converted coordinates is approximately consistent with the convective *B*-*U* plane, where *U* represents the upstream ambient flow and *B* represents the upstream ambient magnetic field. The upstream velocity *U* was not measurable, due to the positive spacecraft potential (Poppe et al., 2012). Fortunately, since the lateral flow velocity when the plasma flow interacts with an ionosphere is approximately laterally symmetric (Jia et al., 2010), we can estimate the direction of *U* by using the direction of the average velocity of lunar ions. This is a reasonable approximation, since the deflection of the ion velocity in the direction perpendicular to the *B*-*U* plane is much smaller than the background flow velocity, based on previous modeling (Jia et al., 2010). The *X* axis in the converted coordinate system is the same as the *X* axis of the SSE coordinates, which is mostly consistent with the lobe magnetic field direction due to the dominated B_x component, so the transformation involves only an angular rotation around the *X* axis. The black curve indicates the trajectory of the satellite, and the orange dot shows the location of the satellite at the beginning of this period. The black circle in the background represents the surface of the Moon.

The ion velocity that ARTEMIS measured significantly rose in the lateral direction during the time period when we observed lunar ions in the *X*-*Y* plane. The parallel velocity V_x was likely provided by acceleration in the near-surface sheath electric field above the lunar surface. Previous studies assumed that the perpendicular velocity V_y was provided by the $-v \times B$ motional electric field (Poppe et al., 2012, 2013). However, in the tenuous magnetotail lobes, the generating mechanism of pickup current associated with mass loading may be reinterpreted (Szegö et al., 2000). Instead, the ambient plasma could be slowed down in the lunar ion region, and the pressure gradients and a curvature of the magnetic field formed to accelerate the source plasma by the magnetic $J \times B$ force (Khurana et al., 2007).

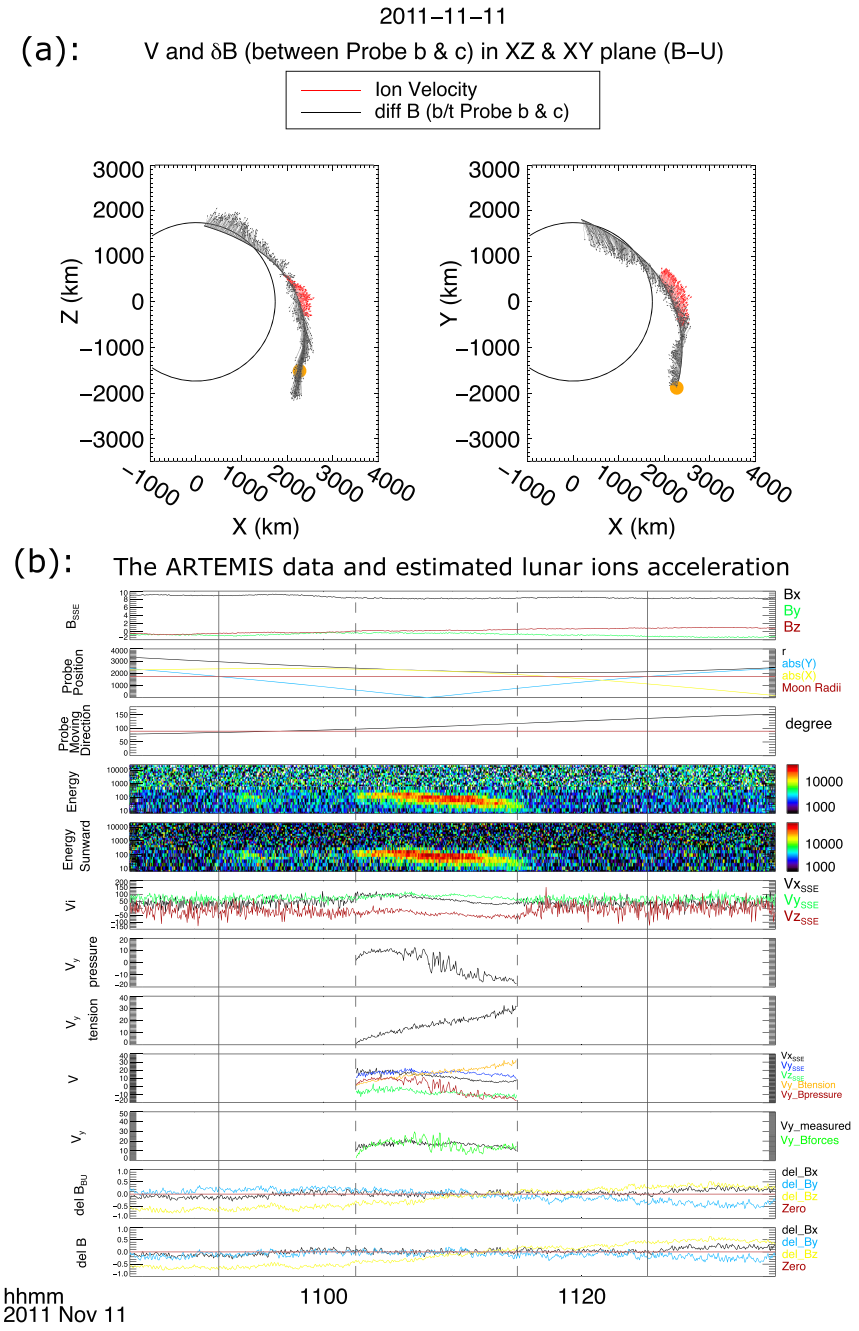

Figure 2. The upper subfigure (a) reveals the ion velocity (red arrows) and magnetic field perturbation (black arrows) measured by ARTEMIS P2 during 10:45–11:35 UTC on 11 November 2011. The arrows are normalized to the unit magnitude and therefore they only indicate the direction. The coordinates are converted from Solar Selenocentric Ecliptic (SSE) into a coordinate system such that the *X*-*Y* plane is aligned with the upstream *B*-*U* plane (see more details in the text). The left represents the *X*-*Z* plane and the right represents the *X*-*Y* (*B*-*U*) plane. The lower subfigure (b) reveals multipanels for the ARTEMIS data and estimation of the lunar ion acceleration by the magnetic tension and pressure in the event of 11 November 2011.

In the *X*-*Y* or (*B*-*U*) plane, the perpendicular component (*Y* direction) of the magnetic field perturbation was positive at the beginning of this event and ended up with negative values, as Figure 2a shows, which corresponds with a mass loading disturbance structure in the *B*-*U* plane. The mass loading of the Moon has an asymmetric disturbance structure along the plasma flow direction. The lunar ionosphere, which is

concentrated on the dayside (Halekas et al., 2018), could produce a mass loading disturbance structure offset toward the dayside, centered on the effective obstacle to the plasma flow. Jia et al. (2010) predicted a similar offset structure for Enceladus, which similarly has a source offset from the Moon. The perturbation was caused by the slowing of the ambient plasma and momentum exchange between the flow and lunar ions. The field lines were thus bent, draped, and diverted around the conducting lunar ion region.

In the *X*-*Z* plane, the bulged magnetic field is produced by the induced currents in the conducting obstacle of the ionosphere, leading to positive B_z in the $+Z$ region and negative B_z in the $-Z$ region in the *X*-*Z* plane as Figure 2a shows, which is consistent with the solid curves in the upper left panel of Figure 1. Meanwhile, a wake is expected to form downstream from the solid obstacle of the Moon, resulting in a potential significant decrease in ambient plasma density. The lack of plasma in the wake region produces a pressure gradient across the wake boundary, as typically seen downstream from the Moon in the solar wind (Zhang et al., 2016) and also analogous to that predicted at Enceladus (Jia et al., 2010). This pressure gradient results in a diamagnetic current (Alken et al., 2011), which perturbs the ambient magnetic field. The resultant magnetic perturbation structure was distorted toward the wake center from the flanks to balance the pressure deficit in the wake (Khurana et al., 2008), which is consistent with the structure that the dashed curves show in Figure 1. In particular, the perpendicular component (*Z* direction) of the magnetic field perturbation at the lower side is toward the $-Z$ direction and the same component at the upper side toward the $+Z$ direction, as Figure 2a shows, correspond with a mass loading structure in which the disturbance is propagated as an Alfvén wave in the plane perpendicular to the *B*-*U* plane. Therefore, the data suggests that the magnetic field perturbation is consistent with a combined mass loading disturbance structure.

In theory, the magnetic tension and pressure generated by the magnetic field perturbation can drive the acceleration of the ions. In order to determine the importance of the magnetic field perturbations on the acceleration of lunar ions, we estimated the components of the magnetic tension force and the magnetic pressure force along ARTEMIS's orbit.

In Figure 2b, the first panel shows the magnetic field measured by P2 during the event of 11 November 2011. The magnetic field was B_x dominated, which indicates that the satellite was in the north tail lobe. The second panel shows the position of the spacecraft, including *r*: the distance of P2 away from the center of the Moon; abs(*X*): the absolute value of *X* of P2's position in SSE coordinates; abs(*Y*): the absolute value of *Y* of P2's position in SSE coordinates. The horizontal line indicates one lunar radius. The third panel shows the angle between the velocity of the satellite and the Sun-Moon line, with a horizontal line for reference at 90°. The spacecraft trajectory was approximately perpendicular to the magnetic field direction during the lunar ion beam time. The fourth and fifth panels are the overall and sunward energy flux spectrum of ions. Two ion beams were detected: a very short and faint one during 10:53–10:55 and a longer one during 11:02:30–11:15:00. In this event, we focus on the long-duration beam for studying the ion acceleration, as in (Poppe et al., 2013). The broad pitch angle distribution of this beam suggests that the lunar ions were sourced from both the near surface and the exosphere (Poppe et al., 2012), so that some of the measured ions have nonzero parallel velocity due to acceleration in the near-surface sheath field. The sixth panel shows the lunar ion velocity in SSE coordinates, which is measured by restricting the velocity direction and energy range in order to reduce the contamination of the background noise. The azimuthal angle is restricted between 260° and 360° and the energy range is between 20 and 176 eV. When ARTEMIS measured the lunar ions during 11:02:30–11:15:00, the velocity moment of ions showed positive V_x, V_y, and negative V_z components. The seventh panel shows the predicted velocity of the lunar ions in the *Y* SSE direction due to acceleration by magnetic pressure, and the eighth panel shows the predicted velocity due to acceleration by magnetic tension. Both of the two variables derived from the discussion in section 2 (the details of the algorithm are described in the supporting information). From the observation, the initial time when ARTEMIS detected the long-period beam was about 11:02:30 UTC, which was marked by the left vertical dashed line in the figure. Therefore, this is the earliest time for the generation of lunar ions with energy above the spacecraft potential in this beam, and no such lunar ions were accelerated before this time point. We acknowledge that there could be ions with energies below the spacecraft potential present before that time. The extreme situation for lunar ions' generation on the dayside should not exceed a radius of the Moon away from the subsolar region along the lateral direction since the photoionization of the exospheric ions only occurs in above the dayside surface. Therefore, we tested this situation as well, which changed the result by no more than a

factor of 2. By assuming the initial perpendicular velocity to be zero, we can estimate the ion velocity at each time point after that by considering the local magnetic forces (tension and pressure) and the perpendicular distance in the Y direction, using Newton's second law. The predicted velocity component in the Y direction due to acceleration by the magnetic tension increases from 0 initially to about 30 km/s at the end of the beam. In contrast, the local magnetic pressure accelerated the lunar ions in the Y direction for a short time in the beginning and then kept slowing them down until the end of the beam. Given the magnitude of the predicted velocities due to acceleration by magnetic forces, the local magnetic field likely played an important role in transferring momentum to the lunar plasma. The ninth panel compares the predicted velocity components due to acceleration by the magnetic tension and pressure with the measured ion velocity (corrected using Equation 4) during the time of the long-duration beam, in SSE coordinates. The orange and red curves are the V_y estimated by the two types of magnetic forces and that measured by ARTEMIS, respectively. The predicted velocity component driven by the magnetic tension (orange color) and that driven by the magnetic pressure (red color) generally match the V_y of lunar ions very well during the whole period of the beam. We note that the former somewhat overestimates, and the latter somewhat underestimates, the actual velocity during the end of the beam. The tenth panel shows that the overall velocity of lunar ions by the combination of the motion driven by magnetic tension and pressure, is consistent with the corrected V_y measured by ARTEMIS, by observing either the magnitude or the shape of the curve. The last two panels show the magnetic field perturbation ARTEMIS measured during this event in the converted coordinate system and in the SSE coordinate system.

3.2. The 29 October 2012 Event

Figure 3a provides an overview of the data from ARTEMIS P1 original measurements of ion velocity and magnetic field difference from ARTEMIS P2 made during 04:45–05:45 UTC on 29 October 2012, when P2 was far upstream from the Moon (~[7, −7, −1] R_U in SSE coordinates) and P1 was above the dayside of the Moon, which is analogous with the first event in Figure 2a. The Moon was at ~[−60, 8, 2] R_E in GSE coordinates.

Similarly, the ion velocity that ARTEMIS measured significantly rose in the lateral direction during the time period when we observed lunar ions in the X-Y plane, as Figure 3a shows. The high pitch angle during this time period verified that the acceleration of lunar ions has a significant perpendicular component (Y direction) and the perpendicular component of the magnetic field perturbation approximately corresponds with a mass loading disturbance structure in the B-U plane. The lunar ionosphere, which is concentrated on the dayside (Halekas et al., 2018), produces a mass loading disturbance structure offset toward the dayside, centered on the effective obstacle to the plasma flow. Jia et al. (2010) predicted a similar offset mass loading disturbance structure for Enceladus, which similarly has a source offset from the Moon. The perturbation was caused by the slowing of the ambient plasma and momentum exchange between the flow and lunar ions. The field lines were thus bent, draped, and diverted around the conducting lunar ion region.

In the X-Z plane, the bulged magnetic field is produced by the induced currents in the conducting obstacle, leading to the variance of B_z across different regions in the X-Z plane as Figure 3a shows, which is consistent with the solid curves in the lower left panel of Figure 1. Meanwhile, a wake forms downstream from the solid obstacle of the Moon, resulting in a significant decrease in ambient plasma density. The lack of plasma in the wake region produces a pressure gradient across the wake boundary, as typically seen downstream from the Moon in the solar wind (Zhang et al., 2016) and also analogous to that predicted at Enceladus (Jia et al., 2010). This pressure gradient results in a diamagnetic current (Alken et al., 2011), which perturbs the ambient magnetic field. The resultant magnetic perturbation structure was distorted toward the wake center from the flanks to balance the pressure deficit in the wake (Khurana et al., 2008), which is consistent with the structure that the dashed curves show in Figure 1. In particular, the perpendicular component (Z direction) of the magnetic field perturbation at the lower side is toward the $+Z$ direction and becomes toward the $-Z$ direction at the upper side, as Figure 3a shows, correspond with a mass loading structure in which the disturbance is propagated as an Alfvén wave in the plane perpendicular to the B-U plane. Therefore, the data suggest that the magnetic field perturbation is consistent with a combined mass loading disturbance and plasma wake structure.

As discussed in the previous section, we estimated the magnetic tension and pressure along ARTEMIS's orbit in order to figure out the influence of the magnetic field perturbations on the acceleration of lunar ions.

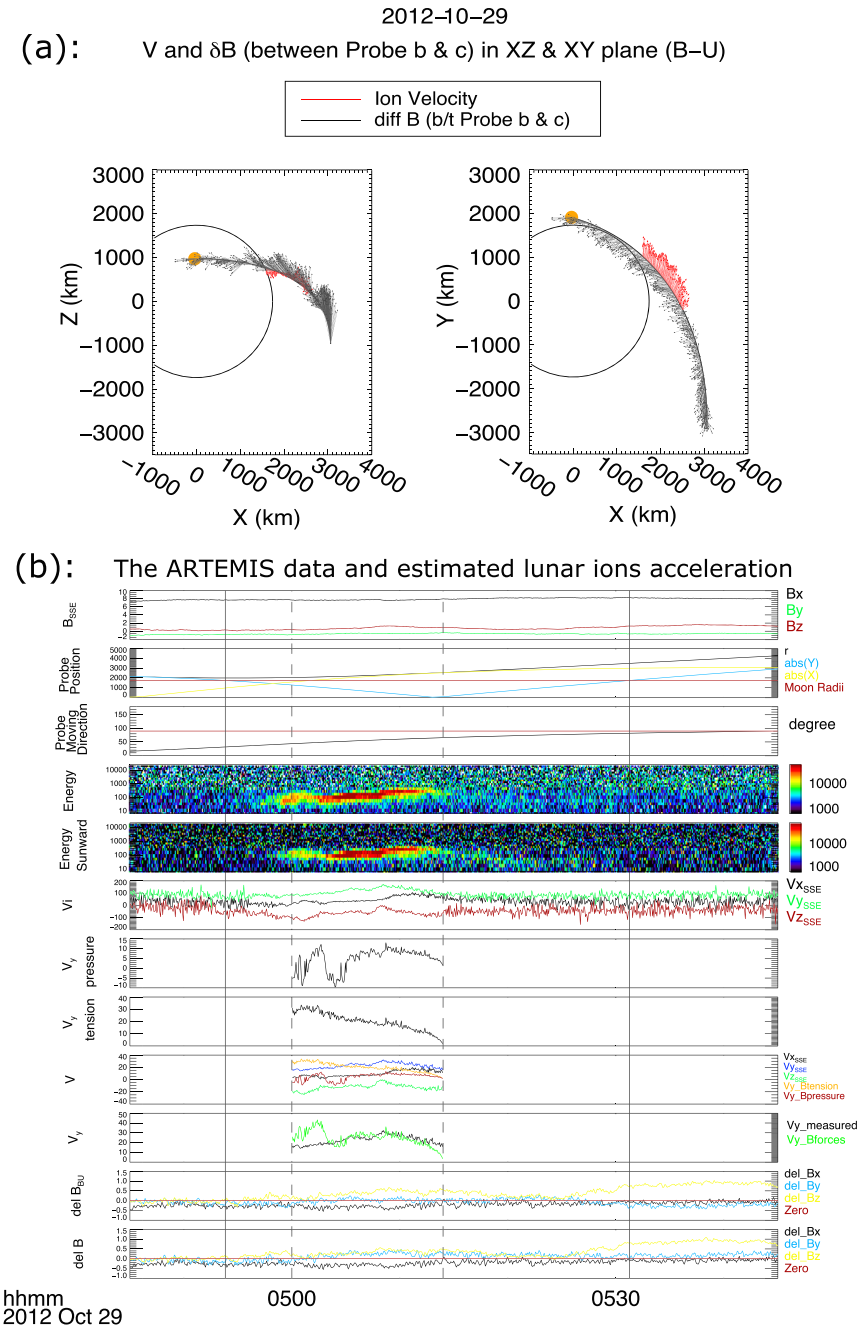

Figure 3. The upper subfigure (a) reveals the ion velocity ARTEMIST P1 measured (red arrows) and the magnetic field perturbation (black arrows) during 04:45–05:45 UTC on 29 October 2012. The arrows are normalized to the unit magnitude and therefore they only indicate the direction. The coordinates are converted from Solar Selenocentric Ecliptic (SSE) coordinate system such that the *X-Y* plane where the average lunar ion velocity and lobe's magnetic field lie on is approximately consistent with the convective *B-U* plane (see more details in the text). The left represents the *X-Z* plane and the right represents the *X-Y* (*B-U*) plane. The lower subfigure (b) reveals multipanels for the ARTEMIS data and estimation of the lunar ion acceleration by the magnetic tension and pressure in the event of 29 October 2012.

In Figure 3b, the variables in each panel correspond with those in Figure 2b. The first panel shows the magnetic field measured by P1 during the event of 29 October 2012. The magnetic field was B_x dominated, which indicates the satellite was in the north tail lobe as well. The second panel shows that the lunar ions were

generated and started to be accelerated near the sub-solar region (about 05:14 UTC), which is marked by the right vertical dashed line. The third panel shows that the spacecraft trajectory was approximately perpendicular to the magnetic field direction when the lunar ions were detected. The fourth and fifth panels are the overall and sunward energy flux spectrum of ions. A long-duration ion beam was detected during 05:00–05:14. We verified that the pitch angle of this beam was approximately around 90°, which suggests that the lunar ions were mainly sourced from the exosphere (Poppe et al., 2012). The sixth panel shows the lunar ion velocity in SSE coordinates, which is measured by restricting the velocity direction and energy range in order to reduce the contamination of the background noise. The azimuthal angle is restricted between 230° and 360° and the energy range is between 50 and 500 eV. When ARTEMIS measured the lunar ions during 05:00–05:14, the velocity moment of ions showed positive V_x, V_y, and negative V_z components, and the magnitude of V_y was larger than that of V_x. The seventh panel shows the predicted velocity of the lunar ions in the Y SSE direction due to acceleration by magnetic pressure, and the eighth panel shows the predicted velocity due to acceleration by magnetic tension. Both of the two variables are derived from the method we have discussed in section 2. From the observation, the initial time when ARTEMIS detected the long-period beam was about 05:14 UTC, which was marked by the right vertical dashed line in the figure. Similarly as the method of the first event, the predicted velocity component in the Y direction due to acceleration by the magnetic tension increases from 0 initially to about 30 km/s at the end of the beam. In contrast, the local magnetic pressure accelerated the lunar ions in the Y direction in the beginning but then decelerated them in a certain of locations during the end of the beam. Given the magnitude of the predicted velocities due to acceleration by magnetic forces, the local magnetic field likely played an important role in transferring momentum to the lunar plasma. The ninth panel compares the predicted velocity components due to acceleration by the magnetic tension and pressure with the measured ion velocity (corrected using Equation 4) during the time of this beam, in SSE coordinates. The orange and red curves are the V_y estimated by the two types of magnetic forces and that measured by ARTEMIS, respectively. The predicted velocity component driven by the magnetic tension (orange color) and that driven by the magnetic pressure (red color) generally match the V_y of lunar ions very well overall the beam. We note that the former somewhat overestimates, and the latter somewhat underestimates, the actual velocity during the end of the beam. The tenth panel shows that the overall velocity of lunar ions by the combination of the motion driven by magnetic tension and pressure is consistent with the corrected V_y measured by ARTEMIS, by observing either the magnitude or the shape of the curve, except a slight overestimation during about 05:00–05:03. This short-period overestimation is possibly produced by three potential causes. First, as the spacecraft moving direction deviated enough from the perpendicular direction, the angle between the spacecraft velocity and the Sun-Moon line reduced down to about 40–50° (as observed in the third panel), which resulted in an appreciable parallel velocity component. Second, the spacecraft started to enter into the wake region during this time period, and the lunar ions generated near the subsolar region could not easily arrive in this wake region by the perpendicular acceleration, which resulted in a lower measurement for the velocity. The lunar ions measured during this short period might be generated from a nearer region which was located between the local place and the subsolar region. The third cause might be due to a dynamic fluctuation of the ambient plasma environment occurring for a short time period. The last two panels show the magnetic field perturbation ARTEMIS measured during this event in the converted coordinate system and in the SSE coordinate system.

4. Summary

In this paper, we showed that the observed magnetic field perturbation produced by the interaction between the lobe plasma flow and the Moon is consistent with the characteristics of a combined mass loading disturbance and plasma wake structure. The resultant magnetic tension and pressure forces should contribute to the acceleration of lunar ions. Our analysis indicates that the conventional pick-up process may not be the dominant ion acceleration process in the tenuous magnetotail lobes.

In conclusion, we have presented two ARTEMIS observations for studying the acceleration of lunar ions in the magnetotail lobes. We investigated the magnetic field perturbation along the trajectory of the satellites and showed that the magnetic structure is consistent with a combined mass loading disturbance and plasma wake structure in the lobes. We made the first-order estimate of the acceleration driven by the magnetic field perturbation, by calculating the magnetic tension and pressure along the trajectory of the satellites above the dayside of the Moon. Our results suggest that magnetic field forces could play a crucial role in accelerating

the lunar ions in the magnetotail lobe. This work can help us to more deeply understand the interaction of lunar ions with the ambient environment in the magnetotail lobes. Such a physical mechanism is also expected to play an important role in the ion acceleration at other moons with a similar ionosphere and analogous ambient environment.

Acknowledgments
We acknowledge support from Solar System Exploration Research Virtual Institute and NASA Contract NAS5-02099. Data Availability Statement All ARTEMIS data are publicly available at NASA's CDAWeb (https://cdaweb.sci.gsfc.nasa.gov) and the ARTEMIS site (http://artemis.ssl. berkeley.edu). We also acknowledge James P. McFadden for Electrostatic Analyzer's data. All ARTEMIS data including Flux Gate Magnetometer and Electrostatic Analyzer's data are publicly available at this site (http://artemis.ssl.berkeley.edu).

References

Alken, P., Maus, S., Richmond, A. D., & Maute, A. (2011). The ionospheric gravity and diamagnetic current systems. *Journal of Geophysical Research*, *116*, https://doi.org/10.1029/2011JA017126

Alvarez-Laguna, A., Ozak, N., Lani, A., Mansour, N. N., Deconinck, H., & Poedts, S. (2018). *A versatile numerical method for the multi-fluid plasma model in partially-and fully-ionized plasmas*, *Journal of Physics: Conference Series* (Vol. 1031, p. 012015). Saint-Malo, France: IOP publishing.

Angelopoulos, V. (2011). The ARTEMIS mission. *Space Science Reviews*, *1*(165), 3–25. https://doi.org/10.1007/s11214-010-9687-2

Auster, H. U., Glassmeier, K. H., Magnes, W., Aydogar, O., Baumjohann, W., Constantinescu, D., et al. (2008). The THEMIS fluxgate magnetometer. *Space Science Reviews*, *141*(1–4), 235–264. https://doi.org/10.1007/s11214-008-9365-9

Bellan, P. M. (2008). *Fundamentals of plasma physics*. Cambridge: Cambridge University Press.

Drell, S. D., Foley, H. M., & Ruderman, M. A. (1965). Drag and propulsion of large satellites in the ionosphere: An Alfvén propulsion engine in space. *Journal of Geophysical Research*, *70*(13), 3131–3145. https://doi.org/10.1029/JZ070i013p03131

Futaana, Y., Machida, S., Saito, Y., Matsuoka, A., & Hayakawa, H. (2003). Moon-related nonthermal ions observed by Nozomi: Species, sources, and generation mechanisms. *Journal of Geophysical Research*, *108*(A1), 1025. https://doi.org/10.1029/2002JA009366

Halekas, J. S., Benna, M., Mahaffy, P. R., Elphic, R. C., Poppe, A. R., & Delory, G. T. (2015). Detections of lunar exospheric ions by the LADEE neutral mass spectrometer. *Geophysical Research Letters*, *42*, 5162–5169. https://doi.org/10.1002/2015GL064746

Halekas, J. S., Delory, G. T., Farrell, W. M., Angelopoulos, V., McFadden, J. P., Bonnell, J. W., et al. (2011). First remote measurements of lunar surface charging from ARTEMIS: Evidence for nonmonotonic sheath potentials above the dayside surface. *Journal of Geophysical Research*, *116*, A07103. https://doi.org/10.1029/2011JA016542

Halekas, J. S., Poppe, A. R., Delory, G. T., Sarantos, M., Farrell, W. M., Angelopoulos, V., & McFadden, J. P. (2012). Lunar pickup ions observed by ARTEMIS: Spatial and temporal distribution and constraints on species and source locations. *Journal of Geophysical Research*, *117*, E06006. https://doi.org/10.1029/2012JE004107

Halekas, J. S., Poppe, A. R., Delory, G. T., Sarantos, M., & McFadden, J. P. (2013). Using ARTEMIS pickup ion observations to place constraints on the lunar atmosphere. *Journal of Geophysical Research: Planets*, *118*, 81–88. https://doi.org/10.1029/2012JE004292

Halekas, J. S., Poppe, A. R., Harada, Y., Bonnell, J. W., Ergun, R. E., & McFadden, J. P. (2018). A tenuous lunar ionosphere in the geomagnetic tail. *Geophysical Research Letters*, *45*, 9450–9459. https://doi.org/10.1029/2018GL079936

Hartle, R. E., & Killen, R. (2006). Measuring pickup ions to characterize the surfaces and exospheres of planetary bodies: Applications to the Moon. *Geophysical Research Letters*, *33*(5), L05201. https://doi.org/10.1029/2005GL024520

Hartle, R. E., Sarantos, M., & Sittler, E. C. (2011). Pickup ion distributions from three-dimensional neutral exospheres. *Journal of Geophysical Research*, *116*, A10101. https://doi.org/10.1029/2011JA016859

Hilchenbach, M., Hovestadt, D., Klecker, B., & Möbius, E. (1992). *Detection of singly ionized energetic lunar pick-up ions upstream of Earth's bow shock. In solar wind seven* (pp. 349–355). Pergamon.

Horányi, M., Szalay, J. R., Kempf, S., Schmidt, J., Grün, E., Srama, R., & Sternovsky, Z. (2015). A permanent, asymmetric dust cloud around the Moon. *Nature*, *522*(7556), 324–326. https://doi.org/10.1038/nature14479

Huang, Z., Tóth, G., Gombosi, T. I., Jia, X., Combi, M. R., Hansen, K. C., et al. (2018). Hall effect in the coma of 67P/Churyumov–Gerasimenko. *Monthly Notices of the Royal Astronomical Society*, *475*(2), 2835–2841. https://doi.org/10.1093/mnras/stx3350

Huebner, W. F., & Mukherjee, J. (2015). Photoionization and photodissociation rates in solar and blackbody radiation fields. *Planetary and Space Science*, *106*, 11–45. https://doi.org/10.1016/j.pss.2014.11.022

Jia, Y. D., Russell, C. T., Khurana, K. K., Toth, G., Leisner, J. S., & Gombosi, T. I. (2010). Interaction of Saturn's magnetosphere and its moons: 1. Interaction between corotating plasma and standard obstacles. *Journal of Geophysical Research*, *115*, A04214, https://doi.org/10.1029/2009JA014630

Kamide, Y., & Chian, A. C. L. (2007). *Handbook of the solar-terrestrial environment*. Springer Science & Business Media. https://doi.org/10.1007/978-3-540-46315-3

Khurana, K. K., Dougherty, M. K., Russell, C. T., & Leisner, J. S. (2007). Mass loading of Saturn's magnetosphere near Enceladus. *Journal of Geophysical Research*, *112*, A08203. https://doi.org/10.1029/2006JA012110

Khurana, K. K., Russell, C. T., & Dougherty, M. K. (2008). Magnetic portraits of Tethys and Rhea. *Icarus*, *193*(2), 465–474. https://doi.org/10.1016/j.icarus.2007.08.005

Kivelson, M. G., Khurana, K. K., Coroniti, F. V., Joy, S., Russell, C. T., Walker, R. J., et al. (1997). The magnetic field and magnetosphere of Ganymede. *Geophysical Research Letters*, *24*(17), 2155–2158. https://doi.org/10.1029/97GL02201

Linker, J. A., Khurana, K. K., Kivelson, M. G., & Walker, R. J. (1998). MHD simulations of Io's interaction with the plasma torus. *Journal Geophysical Research*, *103*(E9), 19,867–19,877. https://doi.org/10.1029/98JE00632

Mall, U., Kirsch, E., Cierpka, K., Wilken, B., Söding, A., Neubauer, F., et al. (1998). Direct observation of lunar pick-up ions near the Moon. *Geophysical Research Letters*, *25*(20), 3799–3802. https://doi.org/10.1029/1998GL900003

McFadden, J. P., Carlson, C. W., Larson, D., Ludlam, M., Abiad, R., Elliott, B., et al. (2008). The THEMIS ESA plasma instrument and in-flight calibration. *Space Science Reviews*, *141*(1–4), 277–302. https://doi.org/10.1007/s11214-008-9440-2

McGrath, M. A., Johnson, R. E., & Lanzerotti, L. J. (1986). Sputtering of sodium on the planet Mercury. *Nature*, *323*(6090), 694–696. https://doi.org/10.1038/323694a0

Neubauer, F. M. (1980). Nonlinear standing Alfvén wave current system at Io: Theory. *Journal of Geophysical Research*, *85*(A3), 1171–1178. https://doi.org/10.1029/JA085iA03p01171

Poppe, A. R., Halekas, J. S., Samad, R., Sarantos, M., & Delory, G. T. (2013). Model-based constraints on the lunar exosphere derived from ARTEMIS pickup ion observations in the terrestrial magnetotail. *Journal of Geophysical Research: Planets*, *118*, 1135–1147. https://doi.org/10.1002/jgre.20090

Poppe, A. R., Samad, R., Halekas, J. S., Sarantos, M., Delory, G. T., Farrell, W. M., et al. (2012). ARTEMIS observations of lunar pick-up ions in the terrestrial magnetotail lobes. *Geophysical Research Letters*, *39*, L17104. https://doi.org/10.1029/2012GL052909

Rubin, M., Koenders, C., Altwegg, K., Combi, M. R., Glassmeier, K. H., Gombosi, T. I., et al. (2014). Plasma environment of a weak comet—Predictions for Comet 67P/Churyumov–Gerasimenko from multifluid-MHD and hybrid models. *Icarus*, *242*, 38–49. https://doi.org/10.1016/j.icarus.2014.07.021

Saito, Y., Yokota, S., Asamura, K., Tanaka, T., Nishino, M. N., Yamamoto, T., et al. (2010). In-flight performance and initial results of plasma energy angle and composition experiment (PACE) on SELENE (Kaguya). *Space Science Reviews*, *154*(1–4), 265–303. https://doi.org/10.1007/s11214-010-9647-x

Sarantos, M., Hartle, R. E., Killen, R. M., Saito, Y., Slavin, J. A., & Glocer, A. (2012). Flux estimates of ions from the lunar exosphere. *Geophysical Research Letters*, *39*, L13101. https://doi.org/10.1029/2012GL052001

Sauer, K., Dubinin, E., Baumgärtel, K., & Bogdanov, A. (1996). Bow shock 'splitting' in bi-ion flows. *Geophysical Research Letters*, *23*(24), 3643–3646. https://doi.org/10.1029/96GL03425

Sillanpää, I., & Johnson, R. E. (2015). The role of ion-neutral collisions in Titan′ s magnetospheric interaction. *Planetary and Space Science*, *108*, 73–86. https://doi.org/10.1016/j.pss.2015.01.007

Simon, S., Kriegel, H., Saur, J., Wennmacher, A., Neubauer, F. M., Roussos, E., et al. (2012). Analysis of Cassini magnetic field observations over the poles of Rhea. *Journal of Geophysical Research*, *117*, A07211. https://doi.org/10.1029/2012JA017747

Stern, S. A. (1999). The lunar atmosphere: History, status, current problems, and context. *Reviews of Geophysics*, *37*(4), 453–491. https://doi.org/10.1029/1999RG900005

Szegö, K., Glassmeier, K. H., Bingham, R., Bogdanov, A., Fischer, C., Haerendel, G., et al. (2000). Physics of mass loaded plasmas. *Space Science Reviews*, *94*(3-4), 429–671. https://doi.org/10.1023/A:1026568530975

Tanaka, T., Saito, Y., Yokota, S., Asamura, K., Nishino, M. N., Tsunakawa, H., et al. (2009). First in situ observation of the Moon-originating ions in the Earth's magnetosphere by MAP-PACE on SELENE (KAGUYA). *Geophysical Research Letters*, *36*, L22106. https://doi.org/10.1029/2009GL040682

Toth, G., Glocer, A., Ma, Y., Najib, D., & Gombosi, T. (2010). Multi-ion magnetohydrodynamics. In Numerical modeling of space plasma flows, Astronum-2009 (Vol. 429, p. 213).

Vasyliūnas, V. M. (2016). Physical origin of pickup currents. *Annales Geophysicae*, *34*(1), 153–156. https://doi.org/10.5194/angeo-34-153-2016

Yokota, S., Saito, Y., Asamura, K., Tanaka, T., Nishino, M. N., Tsunakawa, H., et al. (2009). First direct detection of ions originating from the moon by MAP-PACE IMA onboard SELENE (KAGUYA). *Geophysical Research Letters*, *36*, L11201. https://doi.org/10.1029/2009GL038185

Zhang, H., Khurana, K. K., Kivelson, M. G., Fatemi, S., Holmström, M., Angelopoulos, V., et al. (2016). Alfvén wings in the lunar wake: The role of pressure gradients. *Journal of Geophysical Research: Space Physics*, *121*, 10,698–10,711. https://doi.org/10.1002/2016JA022360

Zhou, X. Z., Angelopoulos, V., Poppe, A. R., & Halekas, J. S. (2013). ARTEMIS observations of lunar pickup ions: Mass constraints on ion species. *Journal of Geophysical Research: Planets*, *118*, 1766–1774. https://doi.org/10.1002/jgre.20125

Zhou, X. Z., Angelopoulos, V., Poppe, A. R., Halekas, J. S., Khurana, K. K., Kivelson, M. G., et al. (2014). Lunar dayside current in the terrestrial lobe: ARTEMIS observations. *Journal of Geophysical Research: Space Physics*, *119*, 3381–3391. https://doi.org/10.1002/2014JA019842

Zieger, B., Opher, M., Tóth, G., Decker, R. B., & Richardson, J. D. (2015). Constraining the pickup ion abundance and temperature through the multifluid reconstruction of the Voyager 2 termination shock crossing. *Journal of Geophysical Research: Space Physics*, *120*, 7130–7153. https://doi.org/10.1002/2015JA021437